AJEV Papers in Press. Published online June 8, 2021.

AJEV PAPERS IN PRESS • AJEV PAPERS IN PRESS

American Journal of Enology and Viticulture (AJEV). doi: 10.5344/ajev.2021.20063
AJEV Papers in Press are peer-reviewed, accepted articles that have not yet been published in a print issue of the journal or edited or formatted, but may be cited by DOI. The final version may contain substantive or nonsubstantive changes.

Research Article

Assessment of Vineyard Water Status by Multispectral and RGB Imagery Obtained from an Unmanned Aerial Vehicle

Patricia López-García,[1] Diego S. Intrigliolo,[2] Miguel A. Moreno,[1] Alejandro Martínez-Moreno,[2] Jose F. Ortega,[1] Eva P. Pérez-Álvarez,[2] and Rocío Ballesteros[1]*

[1]Instituto de Desarrollo Regional (IDR), Universidad de Castilla-La Mancha, Albacete, Spain; and [2]Centro de Edafología y Biología Aplicada del Segura. Consejo Superior de Investigaciones Científicas (CEBAS-CSIC), Murcia, Spain.

*Corresponding author (Rocio.Ballesteros@uclm.es)

Acknowledgments: This research was funded by Ministry of Science, Innovation and Universities, grants number RTC-2017-6365-2, AGL2017-82927-C3-2-R and AGL2017-83738-C3-3-R, and by the Government of Castilla-La Mancha, grant number SBPLY/17/180501/000251. The authors would like to thank the financing with a University Teaching Scholarship (Formación de Profesorado Universitario, FPU). The authors also wish to thank the commercial vineyard owner, the Water User Association "Las Colleras" located in Fuente-Álamo, Albacete, Spain, and the field technicians for their work and involvement in the trial.

Manuscript submitted Oct 7, 2020, revised Jan 14, 2021, March 17, 2021, accepted March 18, 2021

Abstract: Multispectral and conventional cameras, RGB (red, green, blue) imager, onboard unmanned aerial vehicles (UAVs) provide very high spatial, temporal, and spectral resolution data. To evaluate the capacity of these techniques to assess vineyard water status, we carried out a study in a cv. Monastrell vineyard located in southeastern Spain in 2018 and 2019. Several irrigation strategies were applied, including different water quality and quantity regimes. Flights were performed using conventional and multispectral cameras mounted on the UAV throughout the growth cycle. Several visible and multispectral vegetation indices (VIs) were determined from the images with only vegetation (without soil and shadows, among others). Stem water potential was measured by pressure chamber and the water stress integral (Sψ) was obtained along the season. Simple linear regression models that used VIs and

American Journal of Enology and Viticulture (AJEV). doi: 10.5344/ajev.2021.20063
AJEV Papers in Press are peer-reviewed, accepted articles that have not yet been published in a print issue of the journal or edited or formatted, but may be cited by DOI. The final version may contain substantive or nonsubstantive changes.

green cover canopy (GCC) to predict Sψ were tested. The results indicate that visible VIs best correlated with Sψ. The green leaf index (GLI), visible atmospherically resistance index (VARI), and GCC showed the best fits in 2018, with R^2 = 0.8, 0.72, and 0.73, respectively. When the best model developed with the 2018 data was applied to the 2019 data set, the model fit poorly. This suggests that on-ground measurements of vine stress must be taken each growing season to redevelop a model that predicts water stress from UAV based imaging.

Key words: multispectral images, RGB images, stem water potential, UAV, vineyard, water stress

Introduction

Grapevine water status is major determinant for vine performance and wine composition (Jackson and Lombard 1993) potentially affected by many soil and environmental factors interacting with the vine physiology and the vineyard management. In arid and semi-arid areas, irrigation (i.e. the watering regime and its salinity level) plays an important role in determining vine water status (Mirás-Avalos and Intrigliolo 2017).

Efforts have therefore been made to improve water use efficiency and crop yields, moving towards a more sustainable agricultural water management. The concept of precision viticulture (PV) seeks to describe the in-plot vineyard spatial variability to provide recommendations with the objective of improving management efficiency in terms of quality, production and sustainability (Matese and Di Gennaro 2015). One of the techniques that pursues a sustainable agricultural water management is regulated deficit irrigation (RDI), which consists of replacing only part of the potential grapevine evapotranspiration during some previously established phenological periods. Therefore, RDI is a standard practice in Mediterranean viticulture, as an effective means of regulating the water status of

American Journal of Enology and Viticulture (AJEV). doi: 10.5344/ajev.2021.20063
AJEV Papers in Press are peer-reviewed, accepted articles that have not yet been published in a print issue of the journal or edited or formatted, but may be cited by DOI. The final version may contain substantive or nonsubstantive changes.

grapevines under a pressing water scarcity scenario (Romero et al. 2010). The effect of RDI depends on vine phenological stage and plant water stress, as generated by water restrictions and soil and climatic conditions. The application of RDI can mitigate the negative effects of climate change on grapevine productivity and fruit ripening (Buesa et al. 2017), while ensuring the sustainable use of water resources.

Implementation of proper RDI strategies demands the monitoring of grapevine water status; there are different methods to achieve this goal. These include: 1) a more direct determination of plant water status, such as stomatal conductance, stem water potential (Ψ_{stem}), leaf water potential, pre-dawn leaf water potential (Ψ_{pd}), and carbon isotope composition measurements; and 2) sensor monitoring systems collecting a large number of indirect measurements over a period of time, such as transpiration measurements, trunk diameter fluctuations, and leaf and canopy temperatures (Acevedo-Opazo et al. 2008b). Some authors have proposed midday Ψ_{stem} measurements as a significant physiological indicator of water status for irrigated and rain-fed grapevines (Acevedo-Opazo et al. 2010). These measurements are manual, time-consuming, and may be unrepresentative of the spatial variability of water status over the whole farm.

There are many available tools which are used for PV. One of them is the use of remote sensing imagery data from satellites, airplanes, balloons, helicopters, and unmanned aerial vehicles (UAVs) (Boukoberine et al. 2019) to collect spatial data. UAVs with lightweight, high-quality geometric and radiometric sensors allow users to obtain very high spatial (centimetric) and temporal resolution data (Pádua et al. 2017). Spectral reflectance data from on-board sensors have been used to monitor biochemical and biophysical attributes, such as biomass, leaf pigment contents, canopy water status, crop coefficient, and crop evapotranspiration (Zarco-Tejada et al. 2005, Acevedo-Opazo et al. 2008b, Berni et al. 2009, Baluja et al. 2012, Ballesteros et al. 2015). Spectral data are usually employed as a

American Journal of Enology and Viticulture (AJEV). doi: 10.5344/ajev.2021.20063
AJEV Papers in Press are peer-reviewed, accepted articles that have not yet been published in a print issue of the journal or edited or formatted, but may be cited by DOI. The final version may contain substantive or nonsubstantive changes.

mathematical combination of two or more bands to generate vegetation indices (VIs) based on visible or RGB (red, green, blue), red-edge, and near infrared (NIR) regions of the electromagnetic spectrum, among others (Pôças et al. 2015, Romero et al. 2018). The visible part of the spectrum is characterized by low reflectance, due to the strong absorption of foliar pigments such as chlorophyll and carotenoids. The NIR region is characterized by high reflectance, and the thermal domain canopy is characterized by its temperature. As stomata close under pressure stress, transpiration stops and leaf temperatures rise. Thus, leaf or canopy temperatures can be used as a predictor of plant stress (Costa et al. 2010). Recent studies to detect grapevine water stress have used thermal measurements obtained from aerial imagery. Some of them used several multispectral VIs, but few used RGB VIs, as the visible part of the spectrum is characterized by low reflectance (as mentioned above) (Möller et al. 2007, Rodríguez-Pérez et al. 2007, Rossini et al. 2013, Zarco-Tejada et al. 2013, Pôças et al. 2015). Möller et al. (2007) used thermal and visible images to develop models for estimating Ψ_{stem}. However, RGB VIs were not computed and RGB imagery were used only as supporting data. Rodríguez-Pérez et al. (2007), Zarco-Tejada et al. (2013), and Rossini et al. (2013) used the photochemical reflectance index (PRI), suggesting its use as good indicator for water stress monitoring. PRI uses the 530 and 550 wavelengths of the visible region electromagnetic spectrum. Pôças et al. (2015) also used hyperspectral reflectance indices to predict vineyard $\Psi_{pd.}$

Most research studies have adapted methodologies developed in traditional remote sensing methods (using satellite imagery) including the utilized VIs and bands. Nevertheless, the enormous increase of spatial resolution has opened new opportunities to use other bands and VIs, primarily focusing on the visible spectrum (Ballesteros et al. 2018). No reported studies have analyzed the use of VIs derived from the visible bands to predict water status, compared with the traditionally used

American Journal of Enology and Viticulture (AJEV). doi: 10.5344/ajev.2021.20063
AJEV Papers in Press are peer-reviewed, accepted articles that have not yet been published in a print issue of the journal or edited or formatted, but may be cited by DOI. The final version may contain substantive or nonsubstantive changes.

multispectral and thermal VIs. Nevertheless, in this study RGB VIs, in addition to multispectral VIs, were studied as predictors of grapevine water status due to lower cost of RGB cameras and easier photogrammetric treatment, compared with multispectral and thermal products.

Green cover canopy (GCC) is a geometric parameter which provides information about vegetative growth level or canopy vigor. It can be determined from RGB imagery data and is usually related with the leaf area index (LAI), biomass, plant height, and canopy volume, among others (Ballesteros et al. 2015, 2018). Nevertheless, to the best of our knowledge, it has not yet been shown to be related to vine water status. In this study, we evaluate the relationship between GCC and grapevine water status measurements. The objective of this study was to analyze the use of multispectral and RGB VIs and GCC to characterize spatial and temporal variations vineyard water status as a first step of future models that will be developed to estimate vineyard water status according of its location and variety, among others. High frequency multispectral and RGB imaging at high spatial resolution was used to determine VIs as potential predictors of vine water status. The proposed methodology is complementary to field determinations with pressure chamber measurements. In order to obtain a wide range of vine water status conditions, several irrigation regimes were tested including different water salinity levels in order to better taken into account different potential sources of variations for vine water status.

Materials and Methods

Site location and experimental design. The research was undertaken during the 2018 and 2019 growing seasons in a commercial vineyard located in Fuente-Álamo, Albacete, Spain (38º 43’ 43.3’’N, 1º 28’ 12.6’’W; elevation 820 m a.s.l.; see Fig. 1). The soil was sandy loam (55.64% sand, 27.73% silt, and 16.63% clay) with variable depth from 35 to 50 cm. It had 1.2% organic matter, 47.7% active

American Journal of Enology and Viticulture (AJEV). doi: 10.5344/ajev.2021.20063
AJEV Papers in Press are peer-reviewed, accepted articles that have not yet been published in a print issue of the journal or edited or formatted, but may be cited by DOI. The final version may contain substantive or nonsubstantive changes.

118 $CaCO_3$, electrical conductivity (EC) of 0.39 dS/m, pH of 8.86, and bulk density of 1.17 g/cm^3. The
119 irrigation water analysis showed an EC of 1.26 dS/m and pH of 8.37.

120 The climate was defined as continental Mediterranean ("Climate zones. National Geographic
121 Institute (NGI)" 2020), with hot and dry summers and daily maximum summer temperatures close to 40
122 °C, mainly in July and August. The weather station was located 10 km from the experimental plot.
123 Annual rainfall at the experimental site was 406 mm in 2018 and 550 mm in 2019, while rainfall from
124 April to September was 230 mm and 400 mm, respectively. The total annual reference
125 evapotranspiration (ET_o) was 1171 mm in 2018 and 1270 mm in 2019, while ET_o for the growing season
126 was 834 mm and 879 mm, respectively. Growing degree days (GDD) from April to harvest was
127 computed as the sum of the average daily temperature above a threshold of 10 °C (Amerine and Winkler
128 1944). GDD at the harvest was 1904 up to 10th October 2018 and 1868 up to 7th October 2019.

129 The study was performed in a 0.6 ha subplot of a 6.5 ha commercial vineyard. The vines, planted
130 in 2007, were cv. Monastrell on 110R rootstock. They were planted in north–south oriented rows and
131 trained to a double Guyot system on a vertical trellis. The row x vine spacing was 3 m x 1.5 m (2,222
132 vines/ha). Two 2-bud spurs and two 60–90 cm canes were retained during pruning each year. In July,
133 green shoots were trimmed from each grapevine, according to local growing practice. The plot was
134 irrigated with self-compensating dippers spaced by 1 m, with a dripper discharge of 4 l/h.

135 Due to water restrictions under a pressing water scarcity scenario, the annual available water to
136 irrigate was set as 1000 m^3/ha by the water managers in the study area. Six treatments (T1-T6) and four
137 replicates for every treatment were considered as experimental design. Every treatment and replicate
138 were randomly placed along the experimental area (Fig. 1).

American Journal of Enology and Viticulture (AJEV). doi: 10.5344/ajev.2021.20063
AJEV Papers in Press are peer-reviewed, accepted articles that have not yet been published in a print issue of the journal or edited or formatted, but may be cited by DOI. The final version may contain substantive or nonsubstantive changes.

Each replicate involved four rows with 10 vines. The two outer rows were considered as buffers. Also, the most external vines of every row were considered as buffers. The characteristics of different treatments were the following: T1 was rain-fed, T2 was irrigated with standard-quality water, T3 was irrigated adding sulphates (Na_2SO_4 and $MgSO_4$), T4 was irrigated adding sodium chloride (NaCl), and T5 and T6 were irrigated adding sulphates and NaCl respectively, but irrigation events started at veraison. Salts were added to T3, T4, T5, and T6 up to irrigation water reaching an EC of 5 dS/m. Irrigation in T2, T3, and T4 began when Ψ_{stem} reached -0.8 MPa. In 2019 season, the experimental design was simplified, as T5 and T6 were not applied because agronomic and grape quality differences with the others salted treatments (T3 and T4) were not observed. Since the aim of the present study is to correlate different grapevine water status determinations, the fact that T5 and T6 were not used for the 2019 data analysis does not affect the robustness of our results.

Grapevine water status measurement. Grapevine water status was assessed by midday Ψ_{stem} six times in 2018 and seven times in 2019 (Table 1) on two leaves (one leaf per vine) per replicate plot with a pressure chamber (Model 600, PMS Instrument Company, Albany, OR, USA). Previous observations showed that the variation in Ψ_{stem} among leaves of the same grapevines was very low (coefficient of variation lower than 5 %). Therefore, increasing the number of vine measurements instead of increasing the number of Ψ_{stem} determination per vine was performed, as measurements have to be carried out within one hour (Intrigliolo and Castel 2010). Field determinations for Ψ_{stem} were carried out on the same days that aerial images were collected (Table 1), and measurements were always carried out on the same selected vines. Indeed**,** considering the wide range of irrigation treatments explored, vine water status was assessed in a total of 48 and 32 vines, in 2018 and 2019, respectively.

American Journal of Enology and Viticulture (AJEV). doi: 10.5344/ajev.2021.20063
AJEV Papers in Press are peer-reviewed, accepted articles that have not yet been published in a print issue of the journal or edited or formatted, but may be cited by DOI. The final version may contain substantive or nonsubstantive changes.

160 Ψ_{stem} characterizes the grapevine water status at the moment of determination, however, the
161 spectral response of leaves shows the accumulated effect of water deficit duration and intensity from the
162 beginning of the cycle to the moment of determination, represented by water stress integral (S_ψ),
163 computed as the sum of vine water potential measurements during the study period (Buesa et al. 2017).
164 It was calculated, as in equation (1), as the summation of the difference of average of two consecutive
165 measurements of Ψ_{stem} ($\bar{\Psi}_{i,i+1}$) and the least negative value registered during the season (c = -0.35 MPa in
166 both seasons), multiplying it by the number of days between one measurement and the next (n). The
167 possible limitations of the S_ψ may occur when the number of days between two consecutive readings is
168 high. It might have sudden and punctual changes in the water status that may not be noticed, but the
169 water stress integral is the result of the crop water "history", as well as the canopy spectral response. It
170 represents the accumulated water status of the vineyard from the beginning of the cycle until the
171 measurement is taken. Therefore, the main objective of this manuscript is to relate the canopy spectral
172 response with the S_ψ.

$$S_\varphi = \left| \sum_{i=0}^{i=t} \left(\bar{\psi}_{i,i+1} - c \right) n \right| \quad (1)$$

173

174 **Aerial imagery acquisition and processing.** High-resolution multispectral (8 cm ground sample
175 distance; GSD) and RGB (2 cm GSD) images were collected on the same days that Ψ_{stem} was
176 determined (Table 1). The UAV used was a quadcopter md4-1000 (Microdrones Inc., Kreuztal,
177 Germany) mounted with a multispectral SEQUOIA sensor (Parrot, Paris, France) and an RGB SONY
178 ILCE-5100 digital camera (Sony Corporation, Tokyo, Japan). The multispectral SEQUOIA sensor
179 measured four bands: green (550 nm with a 40 nm bandpass filter; BPF), red (660 nm, BPF 40 nm), red-

American Journal of Enology and Viticulture (AJEV). doi: 10.5344/ajev.2021.20063
AJEV Papers in Press are peer-reviewed, accepted articles that have not yet been published in a print issue of the journal or edited or formatted, but may be cited by DOI. The final version may contain substantive or nonsubstantive changes.

edge (735 nm, BPF 10 nm), and NIR (790 nm, BPF 40 nm). The sensor has a 4.8 x 3.6 mm charge coupled device (CCD) and a pixel size of 3.75 x 3.75 μm. The resolution of the image was 1280 x 960 (columns and rows, respectively) with a focal length of 3.98 mm. The sensor of the SONY ILCE-5100 camera was a complementary metal oxide semiconductor (CMOS) Exmor® type APS-C (23.5 x 15.6 mm) with pixel size of 4 x 4 μm. The image size was 6000 x 4000 (columns and rows) and its focal length was 20 mm. Flights were always performed near solar noon at a height of 80 m above ground. Eight targets were uniformly distributed within the flying area for geo-referencing and sensor geometric calibration. The positions of the target centroids were determined using the Leica Global Positioning System (GPS) 1200 (Leica Geosystems AG, Heerbrugg, Switzerland) linked to a Global Navigation Satellite System (GNSS) permanent reference station. The estimated accuracy of the global navigation satellite system real-time kinematic (GNSS-RTK) was 0.01 m in planimetry and 0.015 m in altimetry.

Images were automatically acquired following a flight plan computed using the Microdrones Photogrammetric Flight Planning software (MFLIP) (Hernandez-lopez et al. 2013). Before each flight, radiometric calibration was performed using the Aircalib calibration panel (Airinov, Paris, France) for the multispectral sensor. Blurred images were automatically detected and eliminated (Ribeiro-Gomes et al. 2016). Geomatic products (i.e., orthoimage, digital surface model (DSM), and point cloud) were obtained using the Agisoft Metashape Professional version 1.6.1 software (Agisoft LLC, St. Petersburg, Russia).

Segmentation of well-illuminated vegetation in the orthoimages was performed using a modified version of the LAIC (leaf area index calculation) computer vision software (Córcoles et al. 2013), named GEO-LAIC for RGB imagery treatment and MS-GEO-LAIC for multispectral imagery. This software also made it possible to determine the GCC (Fig. 2). The GCC was computed for each vine

American Journal of Enology and Viticulture (AJEV). doi: 10.5344/ajev.2021.20063
AJEV Papers in Press are peer-reviewed, accepted articles that have not yet been published in a print issue of the journal or edited or formatted, but may be cited by DOI. The final version may contain substantive or nonsubstantive changes.

according to the methodology proposed by Ballesteros et al. (2014). The software used for the extraction of geomatic information for each vine was QGis version 3.4.1 software (QGIS Development Team, 2019, QGIS Geographic Information System. Open Source Geospatial Foundation Project. https://qgis.org).

Calculation of VIs. Sensitiveness of salts treatments on canopy spectral reflectance was previously assessed. There were no significant differences for any seasons and sampling events. Therefore, relationships between water stress integral and considered VIs were studied for all treatments together.

Different VIs were calculated from visible and NIR spectra measured in the RGB and multispectral orthoimages with segmented vegetation. The high resolution images allowed for calculation of a VI for each vine. Band values were computed as the mean of pixel values within its delimited vegetation area with QGis version 3.4.1 software (QGIS Development Team, 2019, QGIS Geographic Information System. Open Source Geospatial Foundation Project. https://qgis.org). Nevertheless, the average of grapevines bands within its replicate plot was band value of each replicate plot of the study, because in the data analysis of this study were used average values for each replicate plot not at the grapevine level.

Statistical analysis. Pearson's correlation coefficient (r) was calculated for the multispectral and RGB VIs listed in Tables 2 and 3. VIs that were highly correlated ($r \geq 0.95$) were not considered. Pearson's correlation analysis was determined between the different VIs and GCC (as predictors) and S_Ψ, throughout the entire growth cycle for the 2018 and 2019 seasons. Simple linear regression models were assessed using as predictors multispectral and RGB VIs with r values of >0.5 in the last dates for 2018 and 2019. The coefficient of determination (R^2) and the relative error (RE) were used to assess the

American Journal of Enology and Viticulture (AJEV). doi: 10.5344/ajev.2021.20063
AJEV Papers in Press are peer-reviewed, accepted articles that have not yet been published in a print issue of the journal or edited or formatted, but may be cited by DOI. The final version may contain substantive or nonsubstantive changes.

performance of the obtained models for each irrigation season. The regression trend line between measured S_ψ and simulated S_ψ, using the VI with the best performance as predictor, was also shown to study the trend of the calibrated model to overestimate or underestimate S_ψ values. Validation was performed in the 2019 data to test the obtained models in 2018; for this, R^2, RE and regression line between measured S_ψ and simulated S_ψ were used to assess the performance.

Results

Accumulated water stress obtained under different treatments. Analyzing the computed S_ψ for each sampling date in the 2018 season (Fig. 3), differences between treatments were not significant until 14th August, even though the first irrigation event was on 2nd July for treatments T2–T4. Differences between T1 (rain-fed grapevines) and the rest of treatments were significant on 14th August (at the beginning of veraison), at 1282 GDD and when the total applied water was 291 mm from rainfall and 55 mm from irrigation. As expected, for that date, T1 showed the highest water stress, with an average S_ψ of 28.9 MPa*days. The lowest S_ψ average value was 19 MPa*days for T2 (irrigated with standard-quality water). The rest of the treatments showed mean values close to 23 MPa*days, in the case of T3 and T4 (irrigated with added sulphates and NaCl, respectively), and close to 26 MPa*days for T5 and T6 (irrigated with added sulphates and NaCl respectively, with watering starting at veraison). In addition, significant differences appeared between T2, T5, and T6, due to the later start of irrigation events. No differences were observed between T2, T3, and T4. Therefore, the results indicate that there were no differences resulting from the two salt types (i.e., T3 *versus* T4 and T5 *versus* T6). In the last two sampling dates, the treatments S_ψ values had the same trend as on 14th August. Differences between T1 and the rest of the treatments were significant on 19th September (at berry ripening) at 1720 GDD

American Journal of Enology and Viticulture (AJEV). doi: 10.5344/ajev.2021.20063
AJEV Papers in Press are peer-reviewed, accepted articles that have not yet been published in a print issue of the journal or edited or formatted, but may be cited by DOI. The final version may contain substantive or nonsubstantive changes.

and when the total applied water reached 337 mm from precipitation and 99 mm from irrigation. T1 showed the highest water stress, with an average S_ψ of 64.3 MPa*days, while the lowest S_ψ average value was 35.3 MPa*days for T2; the rest of treatments showed mean values close to 44 MPa*days for T3 and T4, and close to 50 MPa*days for T5 and T6.

Analyzing the computed S_ψ for each sampling date of the season 2019 (Fig. 4), differences between treatments were not significant until 29th July. In the previous sampling dates, the irrigation treatments had not started yet. Differences between T1 (rain-fed) and T2 (irrigated with standard-quality water) were observed on 29th July (at phenological phase of closed bunch), at 1043 GDD and when the cumulative irrigation water was 15 mm. For that day, T1 showed an average S_ψ value of 12.3 MPa*days and T2 of 7.4 MPa*days. Differences between T1, T2, and T4 with average S_ψ values of 21.9, 12.9, and 18.9 MPa*days were detected, respectively, on 14th August (at veraison) at 1289 GDD and with total applied water of 240 mm from rainfall and 19 mm from irrigation. Differences between T1 and the other treatments were the most significant, with an average S_ψ value of 35.5 MPa*days for T1 and lowest mean value of 19.1 MPa*days for T2 on 28th August (at beginning of berry ripening) at 1468 GDD and with total applied water of 259 mm from rainfall and 40 mm from irrigation. The same trend appeared in the last sampling date, with the highest average value for T1 (47.6 MPa*days) and the lowest mean value for T2 (23.6 MPa*days). Significant differences between T2, T3, and T4 (added salts) were not observed. Therefore, it was shown that irrigation with added salts did not influence the grapevine water status, as was previously observed in 2018.

Correlation of the VIs and analysis of the VIs and GCC with S_ψ. Analysis of Pearson's correlation between the different multispectral VIs for 2018 and 2019 seasons showed that MCARI1, MCARI2, MSAVI, MTVI3, MSR, and SRI had correlation coefficients higher than 0.95, revealing a

American Journal of Enology and Viticulture (AJEV). doi: 10.5344/ajev.2021.20063
AJEV Papers in Press are peer-reviewed, accepted articles that have not yet been published in a print issue of the journal or edited or formatted, but may be cited by DOI. The final version may contain substantive or nonsubstantive changes.

high level of multicollinearity. Therefore, the multispectral VIs considered were NDVI, GI, GNDVI, MCARI, RDVI, and TCARI/OSAVI.

Analysis of Pearson's correlation between the different RGB VIs for 2018 and 2019 seasons showed that γ, NGRDI, Ikaw, ExR, ExB, ExG, ExGR, and RGRI had correlation coefficients higher than 0.95, revealing a high level of multicollinearity. Therefore, the RGB VIs considered were ρ, β, GLI, and VARI.

For selected VIs, Table 4 shows r values for the relationships between the most significant multispectral and RGB VIs (with r values > 0.5 in some dates) with S_ψ in the 2018 season. Generally, r values were higher at the last sampling dates for both types of VIs. Moreover, r values were higher for RGB VIs. The GCC, which is considered a geometric parameter and not such as a spectral VI, showed a good relationship with grapevine water stress. Therefore, canopy growth or grapevine vigor is highly influenced by the accumulated water stress. After Pearson's analysis, we studied simple linear regression models of the multispectral and RGB VIs with r values of >0.5 in the last three or two dates. In the case of multispectral VIs, we considered NDVI, GNDVI, and RDVI. For RGB VIs, we considered GLI, VARI, and the geometric parameter GCC.

Table 5 shows the r values for the relationships between the most significant multispectral and RGB VIs (with r values > 0.5 in some dates) with S_ψ in the 2019 season. Generally, r values were higher in the last sampling dates for both types of VI, as occurred in 2018. Nevertheless, some multispectral VIs only showed r values of >0.5 in the last sampling date (18th September 2019): NDVI, GNDVI, and TCARI/OSAVI. In the case of RGB VIs, as in 2018, GLI, VARI, and GCC had r values of >0.5 in the last three sampling dates (but lower than those in 2018); except for GCC, with a r value of 0.31 on 18th September. GLI also had r values of >0.5 on the 16th and 29th of July.

American Journal of Enology and Viticulture (AJEV). doi: 10.5344/ajev.2021.20063
AJEV Papers in Press are peer-reviewed, accepted articles that have not yet been published in a print issue of the journal or edited or formatted, but may be cited by DOI. The final version may contain substantive or nonsubstantive changes.

Simple linear regression analysis. In order to determine a model to predict grapevine water status, simple linear regression analysis between the multispectral VIs NDVI, GNDVI, and RDVI and the RGB VIs GLI, VARI, and GCC and S_ψ was evaluated for each sampling date in 2018. Table 6 shows the statistical analysis for obtained RGB linear models in the 2018 season. The statistical analysis of multispectral VIs predictors was not detailed as R^2 values were lower than 0.5. Therefore, multispectral VIs offered weak results. According to the r values, the best fits were obtained in the last three sampling dates. The best fit considering RGB VIs as predictor variables was obtained for GLI (R^2 = 0.8 and RE = 8.75%) as a predictor for the last date, 23rd August, at veraison (at 1394 GDD) (Fig. 5a). Generated models using VARI as predictor also had good fits for the last two dates, with $R^2 > 0.5$ and RE > 10%. The generated model including GCC as a predictor showed a good fit, with $R^2 > 0.5$ and RE close to 10%, for the last three dates and with the best fits on 27th July and 14th August with $R^2 = 0.65$ and 0.67, and RE = 9.73 and 10.22%, respectively.

In order to determine a model to predict grapevine water status, simple linear regression analysis between the multispectral VIs NDVI, GNDVI, and TCARI/OSAVI and the RGB VIs GLI, VARI, and GCC and S_ψ was evaluated for each sampling date in 2019. Table 6 shows the statistical analysis for obtained RGB linear models in the 2019 season. Despite the last sampling date, in the case of NDVI and GNDVI, or the last two dates, in the case of TCARI/OSAVI, showing the best fits, neither had $R^2 > 0.5$ and, so, no multispectral model was significant to predict S_ψ (as in 2018), hence the statistical analysis obtained using multispectral VIs as predictors are not shown. In the case of generated models with GCC as predictor, no date had $R^2 > 0.5$. In the case of GLI, the model only showed $R^2 > 0.5$ on 28th August at 1468 GDD (at the beginning of berry ripening). For generated models using VARI as a predictor, only the last two dates had good fit (with $R^2 > 0.5$). In this year, the models did not fit as well as in 2018.

American Journal of Enology and Viticulture (AJEV). doi: 10.5344/ajev.2021.20063
AJEV Papers in Press are peer-reviewed, accepted articles that have not yet been published in a print issue of the journal or edited or formatted, but may be cited by DOI. The final version may contain substantive or nonsubstantive changes.

311 **Validation process.** To evaluate the model generated in 2018, it was applied to the data obtained
312 in 2019. The best linear regression model of the calibration process in 2018 was GLI, with the best
313 statistics on 23rd August (1394 GDD), with R^2 = 0.8 and RE = 8.75%. To validate this model, the
314 calibration equation between GLI and measured S_ψ was applied to GLI on 28th August 2019 with 1468
315 GDD, as it was similar in the GDD at 23rd August 2018. The resulting statistical values were R^2 = 0.59
316 and RE = 33.82%. The model underestimated the S_ψ values when higher S_ψ values were reached (Fig.
317 5b). No multispectral models were validated, as their results were not robust ($R^2 < 0.5$).

318 ## Discussion

319 In both years, differences between the treatments were not clearly observed until mid-August—
320 around veraison—and were mostly found between irrigation regimes, while the application of salt water
321 did not clearly affect grapevine water status. This confirms that the Ψ_{stem} measurement is a good
322 indicator for the watering regime imposed, as recently analyzed in a meta-analysis study (Santesteban et
323 al. 2019). On the other hand, the application of salt water did not affect plant water status, probably as
324 the vineyard's sandy soil avoided the important accumulation of salts in the root-zone. The leaf spectral
325 response was also not affected by the water salinity levels. Thus, data from the different combinations of
326 watering and salinity levels were pooled together when relating vine water status with spectral indexes
327 calculated. Studies determining salinity effects on leaf spectral indexes are still scarce and only recently
328 in citrus trees found that only after 8 seasons of continuous application of salty water from treated waste
329 water it could be detected a differential response in canopy multispectral response (Romero-Trigueros et
330 al. 2017). Comparing the two seasons, the S_ψ values were lower in 2019 than in 2018, due to the lowest
331 Ψ_{stem} values computed in last three sampling dates of 2019. In those dates, irrigation and rainfall events

American Journal of Enology and Viticulture (AJEV). doi: 10.5344/ajev.2021.20063
AJEV Papers in Press are peer-reviewed, accepted articles that have not yet been published in a print issue of the journal or edited or formatted, but may be cited by DOI. The final version may contain substantive or nonsubstantive changes.

were less frequent but with more intensity, highlighting more than 35 mm from rainfall and irrigation registered in previous days to 28th August or more than 100 mm from rainfall in previous days to 18th September. A possible reason that the strongest relationships between water stress and the multispectral and RGB IVs occurred on the last measurement dates is that S_ψ considers accumulated water stress throughout the growing cycle, which probably affected the structural and pigment content of the leaves and, therefore, the spectral response; that is, the source of VIs.

In this study, multispectral and RGB VIs were considered as predictors of S_ψ. The VIs having the strongest relationship with S_ψ were NDVI, GNDVI, RDVI, TCARI/OSAVI, GLI, VARI, and the geometric parameter GCC, where the best results were obtained in the visible domain (i.e., with GLI, VARI, and GCC), with the GLI performance at the last sampling date of 2018 being notable. Few authors have used RGB VIs to predict water status (Möller et al. 2007, Rodríguez-Pérez et al. 2007, Rossini et al. 2013, Zarco-Tejada et al. 2013, Pôças et al. 2015) as the visible part of the spectrum is characterized by low reflectance due to the strong absorption of foliar pigments. Möller et al. (2007) used thermal and visible images to develop models for estimating Ψ_{stem}. Nevertheless, RGB VIs were not computed and RGB imagery were used only as supporting data. Rodríguez-Pérez et al. (2007), Zarco-Tejada et al. (2013), and Rossini et al. (2013) used the photochemical reflectance index (PRI), suggesting its use as good indicator for water stress monitoring. In this study, PRI was not computed because it requires the 530 and 550 wavelengths of the visible region electromagnetic spectrum and the used RGB sensor only provides wavelengths corresponding to red (670 nm), green (550 nm) and blue (470 nm). Pôças et al. (2015) also used hyperspectral reflectance indices to predict vineyard Ψ_{pd}. Their study showed R^2 values ranging from 0.37 to 0.58, having better fit when using VARI ($R^2 = 0.58$). In this study, the best fit of VARI was with 2018's last sampling event for calibration ($R^2 = 0.72$).

American Journal of Enology and Viticulture (AJEV). doi: 10.5344/ajev.2021.20063
AJEV Papers in Press are peer-reviewed, accepted articles that have not yet been published in a print issue of the journal or edited or formatted, but may be cited by DOI. The final version may contain substantive or nonsubstantive changes.

Several studies have used multispectral and thermal VIs to determine water status. Baluja et al. (2012) reported that the highest correlations were obtained for NDVI, MSR, SRI, GNDVI, and TCARI/OSAVI predictors, with R^2 values ranging between 0.58 (GNDVI) and 0.68 (NDVI). In the present study, for both calibration years (2018 and 2019), R^2 values using NDVI and GNDVI as predictors were less accurate (0.42 and 0.49, respectively) for the last sampling date of 2018 (19th September with 1720 GDD). In 2019, the R^2 values of models generated using NDVI, GNDVI, and TCARI/OSAVI were 0.26, 0.41, and 0.46, respectively, for the last sampling date (18th September with 1681 GDD). Poblete et al. (2017) obtained R^2 values for NDVI and GNDVI of 0.35 and 0.31; lower than the obtained values in this study with the 2018 calibration. Romero et al. (2018) obtained R^2 values for NDVI ranging between 0.12 and 0.29 for three sampling dates; lower values than those obtained in the 2018 calibration in this study, and similar to the values obtained in the 2019 calibration. These multispectral VIs can only indirectly detect water status, as they were developed to represent different physiological variables that can change according to different levels of water status (Poblete et al. 2017). In this context, NDVI has been reported to be a good indicator of vegetative vigor, yield, and plant water status (Acevedo-Opazo et al. 2008a), while GNDVI has been reported as a better form to detect chlorophyll pigment concentration, which is modified under stress conditions (Gitelson and Merzlyak 1998).

In the studies carried out by Baluja et al. (2012), Poblete et al. (2017), and Romero et al. (2018), multispectral VIs were related with Ψ_{stem} values, which characterizes the grapevine water status at the moment of determination. Nevertheless, unlike the previous works, the computed VIs in this study were related to S_ψ, which integrates the measured Ψ_{stem} at each sampling date to obtain an accumulated value of water stress, which reflects the effect of water deficit duration and intensity. In the case where

American Journal of Enology and Viticulture (AJEV). doi: 10.5344/ajev.2021.20063
AJEV Papers in Press are peer-reviewed, accepted articles that have not yet been published in a print issue of the journal or edited or formatted, but may be cited by DOI. The final version may contain substantive or nonsubstantive changes.

instantaneous water stress determination is required, thermal imagery is probably more appropriate; although the associated sensor cost and the difficulty of obtaining an accurate geomatic product increases the cost and decreases the applicability of the methodology (Ribeiro-Gomes et al. 2016). Nevertheless, using just RGB products can offer a good solution for determining accumulated water stress, which is a variable used in vineyard water management; particularly for characterizing vineyard zones which may have suffered from different degrees of water stress. Determination of the actual water status by determining Ψ_{stem} is more useful for irrigation scheduling and modulating the irrigation regime, according to the instantaneous water stress suffered by the grapevines.

In the current study, we compared VIs computed from multispectral bands of the Parrot Sequoia and RGB bands from a conventional camera, the Sony ILCE 5100. RGB VIs integrating only information in the visible domain showed better correlations with S_ψ. Moreover, the good performance of these visible VIs was due to the higher spatial resolution, which clearly compensates for the lower reflectance in the visible region, compared with that in NIR and red-edge. The green band is characterized by absorption of radiation by the anthocyanins, water-soluble pigments associated with the resistance of plants to stresses as water deficits (Viña and Gitelson 2011). Blue-band wavelengths refer to a strong absorption by carotenes and xanthophylls which, along with chlorophyll, are used as indicators of physiological states and plant adaptation to stress (Gitelson 2012). Thus, the capability of very-high resolution products in the visible region of the spectrum allows for generating accurate data from the green band, avoiding the need to use multispectral sensors. According to the above results, using RGB VIs to predict S_ψ, instead of traditional multispectral VIs: 1) could reduce costs, as RGB cameras are much cheaper than multispectral ones; 2) could improve the generation of accurate orthoimages, as structure-from-motion software is designed to work with RGB images; 3) sun glint and

American Journal of Enology and Viticulture (AJEV). doi: 10.5344/ajev.2021.20063
AJEV Papers in Press are peer-reviewed, accepted articles that have not yet been published in a print issue of the journal or edited or formatted, but may be cited by DOI. The final version may contain substantive or nonsubstantive changes.

hotspot effects are less pronounced in RGB images than in multispectral ones, which decreases the limitation in the hours of operation (Ortega-Terol et al. 2017); and 4) the point cloud generated is much more accurate, making it possible to obtain the geometric characteristics of the plants, which can improve crop monitoring (Ballesteros et al. 2015).

The GCC is considered to be a geometric parameter which provides information about vegetative growth level or canopy vigor. The GCC is usually related with biomass and plant height but, in this study, GCC was related to S_ψ. Better results were obtained in 2018 than in 2019.

The best-calibrated model, which used GLI and computed S_ψ data for a date of 2018, was validated with GLI data from a date in 2019 with similar GDD. The weak performance of the model generated one year and applied to the next one suggests that it is necessary to make complementary use of field measurements with UAV flights every irrigation season. The implementation of the proposed methodology does not avoid using field measurements, such as pressure chamber measurements. However, it allows applying results obtained in just a few points of the plot to the whole plot. Since water potential determinations have to be carried out within a short time (i.e. one hour) to avoid the differential effects of varying environmental conditions during the day, the procedure here developed could be used to map the entire vineyard water status variability from a few on-the-ground point determinations. This is of particular interest for both, obtaining a more representative evaluation of the entire vineyard water status and to determine different zones within the vineyard. Nevertheless, obtaining aerial images from veraison to senesce may be enough to monitor differences in water status. All calibrated models for both seasons showed better performance in the last sampling dates, when the fruit development was at veraison and differences in water status were observed. This was more significative for GLI performance, as it has been previously mentioned, on 23rd August 2018 when 1394

American Journal of Enology and Viticulture (AJEV). doi: 10.5344/ajev.2021.20063
AJEV Papers in Press are peer-reviewed, accepted articles that have not yet been published in a print issue of the journal or edited or formatted, but may be cited by DOI. The final version may contain substantive or nonsubstantive changes.

GDD. However, field measurements are necessary to quantify it. It is important to highlight that monitoring water status depends on the rain regime, irrigation scheduling, and crop development, making it necessary to determine the most appropriate flight stating date for every individual case.

Conclusion

The use of RGB cameras onboard a UAV platform allowed us to obtain high spatial resolution images for the monitoring of grapevine water status with better results than when using (more complex) multispectral images. This, together with occasional pressure chamber measurements, permits the monitoring of water status throughout the whole vineyard. The use of conventional RGB cameras increases the applicability of the proposed methodology, due to the lower cost of the system and easier photogrammetric treatment, compared with multispectral and thermal products. Moreover, the results from 2018 showed that canopy growth (represented by GCC obtained from the RGB camera) also had a good correlation with grapevine water status; therefore, it can be used as predictor for the mid-term effects of water deficit.

Because of the poor results obtained when applying a model calibrated for one year to another season, it can be concluded that it is necessary to generate a new empirical model for every season. Nevertheless, only flights close to veraison were necessary in the case study, reducing the number of required flights and, therefore, the cost of application.

Future advances will be focused on implementing other statistical regression models, such as machine learning techniques, to enhance the obtained fits. Furthermore, more efforts will be made to predict the water status in a specific date of any year using a previous generalizable calibrated model by extending the number of analyzed seasons.

American Journal of Enology and Viticulture (AJEV). doi: 10.5344/ajev.2021.20063
AJEV Papers in Press are peer-reviewed, accepted articles that have not yet been published in a print issue of the journal or edited or formatted, but may be cited by DOI. The final version may contain substantive or nonsubstantive changes.

Literature Cited

Acevedo-Opazo C, Tisseyre B, Guillaume S, Ojeda H. 2008a. The potential of high spatial resolution information to define within-vineyard zones related to vine water status. Precis Agric 9:285–302.

Acevedo-Opazo C, Tisseyre B, Ojeda H, Ortega-Farias S, Guillaume S. 2008b. Is it possible to assess the spatial variability of vine water status? OENO One 42:203–219.

Acevedo-Opazo C, Ortega-Farias S, Fuentes S. 2010. Effects of grapevine (Vitis vinifera L.) water status on water consumption, vegetative growth and grape quality: An irrigation scheduling application to achieve regulated deficit irrigation. Agric Water Manag 97:956–964.

Amerine MA, Winkler AJ. 1944. Composition and quality of musts and wines of California grapes. Hilgardia A J Agric Sci Publ by Calif Agric Exp Stn 15:184.

Baggiolini M. 1952. Les stades repères dans le développment annuel de la vigne et leur utilisation pratique. Rev Rom d'Agriculture d'Arboriculture 8:4–6.

Ballesteros R, Ortega JF, Hernández D, Moreno MA. 2014. Applications of georeferenced high-resolution images obtained with unmanned aerial vehicles. Part I: Description of image acquisition and processing. Precis Agric 15:579–592.

Ballesteros R, Ortega JF, Hernández D, Moreno MÁ. 2015. Characterization of Vitis vinifera L. canopy using unmanned aerial vehicle-based remote sensing and photogrammetry techniques. Am J Enol Vitic 66:120–129.

Ballesteros R, Ortega JF, Hernandez D, Moreno MA. 2018. Onion biomass monitoring using UAV-based RGB imaging. Precis Agric 19:840–857.

Baluja J, Diago MP, Balda P, Zorer R, Meggio F, Morales F, Tardaguila J. 2012. Assessment of vineyard water status variability by thermal and multispectral imagery using an unmanned aerial vehicle (UAV). Irrig Sci 30:511–522.

Berni J, Zarco-Tejada PJ, Suárez L, Fereres E. 2009. Thermal and narrowband multispectral remote sensing for vegetation monitoring from an unmanned aerial vehicle. IEEE Trans Geosci Remote Sens 47:722–738.

Boukoberine MN, Zhou Z, Benbouzid M. 2019. A critical review on unmanned aerial vehicles power supply and energy management: Solutions, strategies, and prospects. Appl Energy 255:113823.

Buesa I, Pérez D, Castel J, Intrigliolo DS, Castel JR. 2017. Effect of deficit irrigation on vine performance and grape composition of Vitis vinifera L. cv. Muscat of Alexandria. Aust J Grape Wine Res 23:251–259.

Chen JM. 1996. Evaluation of vegetation indices and a modified simple ratio for boreal applications.

American Journal of Enology and Viticulture (AJEV). doi: 10.5344/ajev.2021.20063
AJEV Papers in Press are peer-reviewed, accepted articles that have not yet been published in a print issue of the journal or edited or formatted, but may be cited by DOI. The final version may contain substantive or nonsubstantive changes.

Can J Remote Sens 22:229–242.

Climate zones. National Geographic Institute (NGI). 2020. as found on the website (https://www.ign.es/espmap/mapas_clima_bach/pdf/Clima_Mapa_1_2texto.pdf).

Córcoles JI, Ortega JF, Hernández D, Moreno MA. 2013. Estimation of leaf area index in onion (Allium cepa L.) using an unmanned aerial vehicle. Biosyst Eng 115:31–42.

Costa JM, Grant OM, Chaves MM. 2010. Use of thermal imaging in viticulture: current application and future prospects. *In* Methodologies and Results in Grapevine Research. S Delrot (ed.), pp. 136–147. Springer Science+Business Media B.V.

Daughtry CST, Walthall CL, Kim MS, de Colstoun EB, McMurtrey III JE. 2000. Estimating corn leaf chlorophyll concentration from leaf and canopy reflectance. Remote Sens Environ 74:229–239.

Gitelson AA. 2012. Non-destructive estimation of foliar pigment (chlorophylls, carotenoids and anthocyanins) contents: Evaluating a semianalytical three-band model.

Gitelson AA, Merzlyak MN. 1998. Remote sensing of chlorophyll concentration in higher plant leaves. Adv Sp Res 22:689–692.

Gitelson AA, Kaufman YJ, Stark R, Rundquist D. 2002. Novel algorithms for remote estimation of vegetation fraction. Remote Sens Environ 80:76–87.

Haboudane D, Miller JR, Tremblay N, Zarco-Tejada PJ, Dextraze L. 2002. Integrated narrow-band vegetation indices for prediction of crop chlorophyll content for application to precision agriculture. Remote Sens Environ 81:416–426.

Haboudane D, Miller JR, Pattey E, Zarco-Tejada PJ, Strachan IB. 2004. Hyperspectral vegetation indices and novel algorithms for predicting green LAI of crop canopies: Modeling and validation in the context of precision agriculture. Remote Sens Environ 90:337–352.

Hernandez-lopez D, Felipe-garcia B, Gonzalez-aguilera D, Arias-perez B. 2013. An automatic approach to UAV flight planning and control for photogrammetric applications: A test case in the Asturias region (Spain). Photogramm Eng Remote Sens 79:87–98.

Intrigliolo DS, Castel JR. 2010. Response of grapevine cv. "Tempranillo" to timing and amount of irrigation: Water relations, vine growth, yield and berry and wine composition. Irrig Sci 28:113–125.

Jackson DI, Lombard PB. 1993. Environmental and Management Practices Affecting Grape Composition and Wine Quality - A Review. Am J Enol Vitic 44.

Jordan CF. 1969. Derivation of leaf area index from quality of light on the forest floor. Ecology 50:663–666.

American Journal of Enology and Viticulture (AJEV). doi: 10.5344/ajev.2021.20063
AJEV Papers in Press are peer-reviewed, accepted articles that have not yet been published in a print issue of the journal or edited or formatted, but may be cited by DOI. The final version may contain substantive or nonsubstantive changes.

505 Kawashima S, Nakatani M. 1998. An algorithm for estimating chlorophyll content in leaves. Ann Bot
506 81:49–54.

507 Louhaichi M, Borman MM, Johnson DE. 2001. Spatially located platform and aerial photography for
508 documentation of grazing impacts on wheat. Geocarto Int 16:65–70.

509 Mao W, Wang Y, Wang Y. 2003. Real-time detection of between-row weeds using machine vision.
510 ASAE Annu Meet 300.

511 Matese A, Di Gennaro SF. 2015. Technology in precision viticulture: A state of the art review. Int J
512 Wine Res 7:69–81.

513 Mirás-Avalos JM, Intrigliolo DS. 2017. Grape Composition under Abiotic Constrains: Water Stress and
514 Salinity. Front Plant Sci 8:851.

515 Möller M, Alchanatis V, Cohen Y, Meron M, Tsipris J, Naor A, Ostrovsky V, Sprintsin M, Cohen S.
516 2007. Use of thermal and visible imagery for estimating crop water status of irrigated grapevine. J
517 Exp Bot 58:827–838.

518 Ortega-Terol D, Hernandez-Lopez D, Ballesteros R, Gonzalez-Aguilera D. 2017. Automatic hotspot and
519 sun glint detection in UAV multispectral images. Sensors (Switzerland) 17:1–16.

520 Pádua L, Vanko J, Hruška J, Adão T, Sousa JJ, Peres E, Morais R. 2017. UAS, sensors, and data
521 processing in agroforestry: a review towards practical applications. Int J Remote Sens 38:2349–
522 2391.

523 Poblete T, Ortega-Farías S, Moreno MA, Bardeen M. 2017. Artificial neural network to predict vine
524 water status spatial variability using multispectral information obtained from an unmanned aerial
525 vehicle (UAV). Sensors 17.

526 Pôças I, Rodrigues A, Gonçalves S, Costa PM, Gonçalves I, Pereira LS, Cunha M. 2015. Predicting
527 grapevine water status based on hyperspectral reflectance vegetation indices. Remote Sens
528 7:16460–16479.

529 Qi J, Chehbouni A, Huete AR, Kerr YH, Sorooshian S. 1994. A modified soil adjusted vegetation index.
530 Remote Sens Environ 48:119–126.

531 Ribeiro-Gomes K, Hernandez-Lopez D, Ballesteros R, Moreno MA. 2016. Approximate georeferencing
532 and automatic blurred image detection to reduce the costs of UAV use in environmental and
533 agricultural applications. Biosyst Eng 151:308–327.

534 Rodríguez-Pérez JR, Riaño D, Carlisle E, Ustin S, Smart DR. 2007. Evaluation of hyperspectral
535 reflectance indexes to detect grapevine water status in vineyards. Am J Enol Vitic 58:302–317.

536 Romero-Trigueros C, Nortes PA, Alarcón JJ, Hunink JE, Parra M, Contreras S, Droogers P, Nicolás E.
537 2017. Effects of saline reclaimed waters and deficit irrigation on Citrus physiology assessed by

American Journal of Enology and Viticulture (AJEV). doi: 10.5344/ajev.2021.20063
AJEV Papers in Press are peer-reviewed, accepted articles that have not yet been published in a print issue of the journal or edited or formatted, but may be cited by DOI. The final version may contain substantive or nonsubstantive changes.

538 UAV remote sensing. Agric Water Manag 183:60–69.

539 Romero M, Luo Y, Su B, Fuentes S. 2018. Vineyard water status estimation using multispectral imagery
540 from an UAV platform and machine learning algorithms for irrigation scheduling management.
541 Comput Electron Agric 147:109–117.

542 Romero P, Fernández-Fernández JI, Martinez-Cutillas A. 2010. Physiological thresholds for efficient
543 regulated deficit-irrigation management in winegrapes grown under semiarid conditions. Am J Enol
544 Vitic 61:300–312.

545 Rossini M, Fava F, Cogliati S, Meroni M, Marchesi A, Panigada C, Giardino C, Busetto L, Migliavacca
546 M, Amaducci S, et al. 2013. Assessing canopy PRI from airborne imagery to map water stress in
547 maize. ISPRS J Photogramm Remote Sens 86:168–177.

548 Roujean J-L, Breon F-M. 1995. Estimating PAR absorbed by vegetation from bidirectional reflectance
549 measurements. Remote Sens Environ 51:375–384.

550 Rouse J, Haas R, Schell J, Deering D, Harlan J. 1974. Monitoring the vernal advancement and
551 retrogradation (Green-wave effect) of natural vegetation. United States.

552 Saberioon MM, Amin MSM, Anuar AR, Gholizadeh A, Wayayok A, Khairunniza-bejo S. 2014.
553 Assessment of rice leaf chlorophyll content using visible bands at different growth stages at both
554 the leaf and canopy scale. Int J Appl Earth Obs Geoinf 32:35–45.

555 Santesteban LG, Miranda C, Marín D, Sesma B, Intrigliolo DS, Mirás-Avalos JM, Escalona JM,
556 Montoro A, de Herralde F, Baeza P, et al. 2019. Discrimination ability of leaf and stem water
557 potential at different times of the day through a meta-analysis in grapevine (Vitis vinifera L.). Agric
558 Water Manag 221:202–210.

559 Viña A, Gitelson AA. 2011. Sensitivity to foliar anthocyanin content of vegetation indices using green
560 reflectance. IEEE Geosci Remote Sens Lett 8:464–468.

561 Zarco-Tejada PJ, Berjón A, López-Lozano R, Miller, J.R., Martín P, Cachorro V, González MR, de
562 Frutos A. 2005. Assessing vineyard condition with hyperspectral indices: Leaf and canopy
563 reflectance simulation in a row-structured discontinuous canopy. Remote Sens Environ 99:271–
564 287.

565 Zarco-Tejada PJ, González-Dugo V, Williams LE, Suárez L, Berni JAJ, Goldhamer D, Fereres E. 2013.
566 A PRI-based water stress index combining structural and chlorophyll effects: Assessment using
567 diurnal narrow-band airborne imagery and the CWSI thermal index. Remote Sens Environ 138:38–
568 50.

569

American Journal of Enology and Viticulture (AJEV). doi: 10.5344/ajev.2021.20063

Table 1 Dates of Ψ_{stem} measurements and flights, calculated growing degree days (GDD), and accumulated applied water by rainfall and irrigation in the studied vineyard cv. Monastrell located in southeastern Spain in 2018 and 2019 seasons.

	Sampling date	DOY	Growth stage (Baggiolini scale[a])	GDD	Applied water (mm)	
					Rainfall	Irrigation
Season 2018	15th June	166	H-I: flowering	396	264	0
	2nd July	183	J: fruit set	614	288	4
	27th July	208	L: closed bunch	989	288	44
	14th August	226	M: beginning veraison	1282	291	55
	23rd August	235	M: veraison	1394	307	70
	19th September	262	N: berry ripening	1720	337	99
Season 2019	19th June	170	J: beginning fruit set	453	233	0
	4th July	185	J: ended fruit set	665	233	0
	16th July	197	K: berry pea size	849	240	0
	29th July	210	L: closed bunch	1043	240	15
	14th August	226	M: veraison	1289	240	19
	28th August	240	N: beginning berry ripening	1468	259	40
	18th September	261	N: berry ripening	1681	428	56

DOY: days over year; GDD: accumulated growing degree days
[a]Baggiolini scale: (Baggiolini 1952)

American Journal of Enology and Viticulture (AJEV). doi: 10.5344/ajev.2021.20063
AJEV Papers in Press are peer-reviewed, accepted articles that have not yet been published in a print issue of the journal or edited or formatted, but may be cited by DOI. The final version may contain substantive or nonsubstantive changes.

Table 2 Multispectral VIs used in the present study calculated using the Parrot Sequoia sensor's set of bands. These VIs were calculated for vineyard cv. Monastrell located in southeastern Spain in 2018 and 2019 seasons.

	Index	Equation	References
GI	Greenness Index	R_{550}/R_{670}	(Zarco-Tejada et al. 2005)
GNDVI	Green Normalized Difference Vegetation Index	$\frac{R_{800}-R_{550}}{R_{800}+R_{550}}$	(Gitelson and Merzlyak 1998)
MCARI	Modified Chlorophyll Absorption in Reflectance Index	$[(R_{700}-R_{670})-0.2*(R_{700}-R_{550})]*(\frac{R_{700}}{R_{670}})$	(Daughtry et al. 2000)
MCARI1	Modified Chlorophyll Absorption in Reflectance Index 1	$1.2*[2.5*(R_{800}-R_{670})-1.3*(R_{800}-R_{550})]$	(Haboudane et al. 2004)
MCARI2	Modified Chlorophyll Absorption in Reflectance Index 2	$\frac{1.2*[2.5*(R_{800}-R_{670})-1.3*(R_{800}-R_{550})]}{\sqrt{(2*R_{800}+1)^2-6*(R_{800}-5*R_{670})-0.5}}$	(Haboudane et al. 2004)
MSAVI	Improved Soil-Adjusted Vegetation Index	$\frac{(2*R_{800}+1-\sqrt{(2*R_{800}+1)^2-8*(R_{800}-R_{670})}}{2}$	(Qi et al. 1994)
MSR	Modified Simple Ratio	$\frac{\frac{R_{800}}{R_{670}}-1}{\sqrt{\frac{R_{800}}{R_{670}}+1}}$	(Chen 1996)
MTVI3	Modified Triangular Vegetation Index	$1.2*[1.2*(R_{800}-R_{550})-2.5*(R_{670}-R_{550})]$	(Rodríguez-Pérez et al. 2007)
NDVI	Normalized Difference Vegetation Index	$\frac{R_{800}-R_{670}}{R_{800}+R_{670}}$	(Rouse et al. 1974)
TCARI/ OSAVI	Transformed Chlorophyll Absorption in Reflectance Index/Optimized Soil-Adjusted Vegetation Index	$\frac{3*[(R_{700}-R_{670})-0.2*(R_{700}-R_{550})*(R_{700}/R_{670}}{(1+0.16)*(R_{800}-R_{670})/(R_{800}+R_{670}+0.16)}$	(Haboudane et al. 2002)
SRI	Simple Ratio Index	$\frac{R_{800}}{R_{550}}$	(Jordan 1969)
RDVI	Renormalized Difference Vegetation Index	$\frac{R_{800}-R_{670}}{\sqrt{R_{800}+R_{670}}}$	(Roujean and Breon 1995)

American Journal of Enology and Viticulture (AJEV). doi: 10.5344/ajev.2021.20063
AJEV Papers in Press are peer-reviewed, accepted articles that have not yet been published in a print issue of the journal or edited or formatted, but may be cited by DOI. The final version may contain substantive or nonsubstantive changes.

Table 3 RGB VIs used in the present study calculated using the SONY-ILCE 5100 sensor's set of bands. These VIs were calculated for vineyard cv. Monastrell located in southeastern Spain in 2018 and 2019 seasons.

	Index	Equation	References
ρ	Normalized red	$\frac{R}{R+G+B}$	(Saberioon et al. 2014)
γ	Normalized green	$\frac{G}{R+G+B}$	(Saberioon et al. 2014)
β	Normalized blue	$\frac{B}{R+G+B}$	(Saberioon et al. 2014)
NGRDI	Normalized Green Red Difference Index	$\frac{\gamma-\beta}{\gamma+\beta}$	(Gitelson et al. 2002)
Ikaw	Kawashima Index	$\frac{\rho-\beta}{\rho+\beta}$	(Kawashima and Nakatani 1998)
ExR	Excess Red Vegetation Index	$1.4*\rho-\gamma$	(Mao et al. 2003)
ExB	Excess Blue Vegetation Index	$1.4*\beta-\gamma$	(Mao et al. 2003)
ExG	Excess Green Vegetation Index	$2*\gamma-\rho-\beta$	(Mao et al. 2003)
ExGR	Excess Green minus Excess Red Index	$ExG-ExR$	(Mao et al. 2003)
RGRI	Red Green Ratio Index	$\frac{\rho}{\gamma}$	(Saberioon et al. 2014)
GLI	Green Leaf Index	$\frac{2*\gamma-\rho-\beta}{2*\gamma+\rho+\beta}$	(Louhaichi et al. 2001)
VARI	Visible Atmospherically Resistance Index	$\frac{\gamma-\rho}{\gamma+\rho-\beta}$	(Gitelson et al. 2002)

Table 4 Pearson's correlation coefficients for the relationships between the most significant VIs with S_ψ (MPa*days) in the 2018 season for the studied vineyard cv. Monastrell located in southeastern Spain.

	Multispectral VIs			RGB VIs		
	NDVI	**GNDVI**	**RDVI**	**GLI**	**VARI**	**GCC**
15th June 2018	-0.06	-0.05	-0.26	0.19	0.07	-0.23
2nd July 2018				-0.19	-0.16	-0.43
27th July 2018	-0.27	-0.26	-0.17	-0.32	**-0.56**	**-0.81**
14th August 2018	**-0.62**	**-0.66**	**-0.67**	**-0.70**	**-0.75**	**-0.82**
23rd August 2018	**-0.65**	**-0.67**	**-0.66**	**-0.89**	**-0.85**	**-0.85**
19th September 2018	**-0.64**	**-0.7**	**-0.59**			

American Journal of Enology and Viticulture (AJEV). doi: 10.5344/ajev.2021.20063
AJEV Papers in Press are peer-reviewed, accepted articles that have not yet been published in a print issue of the journal or edited or formatted, but may be cited by DOI. The final version may contain substantive or nonsubstantive changes.

Table 5 Pearson's correlation coefficients for the relationships between the most significant VIs with S_ψ (MPa*days) in the 2019 season for the studied vineyard cv. Monastrell located in southeastern Spain.

	Multispectral VIs			RGB VIs		
	NDVI	**GNDVI**	**TCARI/OSAVI**	**GLI**	**VARI**	**GCC**
19th June 2019	1.2e-3	0.11	0.09	-0.24	-0.22	0.08
4th July 2019	-0.28	-0.01	0.11	-0.41	-0.35	-0.37
16th July 2019	-0.37	-0.3	0.35	**-0.53**	-0.39	-0.4
29th July 2019	-0.32	-0.26	0.32	**-0.58**	-0.38	-0.34
14th August 2019	-0.44	-0.34	0.35	**-0.5**	**-0.67**	**-0.53**
28th August 2019	-0.35	-0.4	**0.63**	**-0.77**	**-0.75**	**-0.57**
18th September 2019	**-0.51**	**-0.64**	**0.68**	-0.48	**-0.73**	-0.31

Table 6 Statistics of generated simple linear regression models using the most significant RGB VIs* as predictors in the 2018 and 2019 seasons for the studied vineyard cv. Monastrell located in southeastern Spain.

RGB VIs and GCC in 2018 season	**GLI**				**VARI**				**GCC**			
	R^2	**RE (%)**	**a**	**b**	**R^2**	**RE (%)**	**a**	**b**	**R^2**	**RE (%)**	**a**	**b**
15th June 2018	0.04	9.14	0.83	0.34	3.5e-3	9.29	0.27	0.42	0.05	9.06	-5.9e-3	0.48
2nd July 2018	0.04	15.27	-9.25	6.62	0.03	15.35	-5.1	5.55	0.18	14.06	-0.11	6.57
27th July 2018	0.11	15.65	-83	23.9	0.32	13.66	-115	24.56	**0.65**	**9.73**	-0.74	22.68
14th August 2018	0.48	12.79	-273.75	49.94	**0.56**	**11.78**	-209.08	37.05	**0.67**	**10.22**	-1.49	45.06
23rd August 2018	**0.8**	**8.75**	-479.01	74.42	**0.72**	**10.35**	-346.75	46.1	**0.73**	**10.19**	-1.78	57.81
RGB VIs and GCC in 2019 season	**GLI**				**VARI**				**GCC**			
	R^2	**RE (%)**	**a**	**b**	**R^2**	**RE (%)**	**a**	**b**	**R^2**	**RE (%)**	**a**	**b**
19th June 2019	0.06	26.67	-4.81	1.04	0.05	26.74	-3.03	0.64	6.7e-3	27.37	6.8e-3	0.43
4th July 2019	0.17	40.03	-57.03	12.02	0.13	41	-47.81	7.69	0.13	40.75	-0.17	5.45
16th July 2019	0.29	28.76	-116.12	21.01	0.15	31.43	-46.51	10.17	0.16	31.31	-0.32	10.2
29th July 2019	0.32	24.38	-252.7	37.58	0.15	27.33	-84.73	15.48	0.11	27.87	-0.39	15.26
14th August 2019	0.25	22.85	-433.9	52.23	0.46	19.43	-297.98	27.67	0.28	22.41	-0.79	30.71
28th August 2019	**0.59**	**18.32**	-590.43	94.73	**0.55**	**19.24**	-434.1	47.11	0.33	23.53	-2.52	53.22
18th September 2019	0.23	28.88	-505.38	81.4	**0.55**	**22.02**	-986.13	49.9	0.09	31.22	-1.36	47.96

R^2: coefficient of determination; RE: relative error; a and b: coefficients of the generated model's equation ($S_\psi = ax + b$)
*: statistics of generated simple linear regression models using multispectral VIs as predictors are not shown because all analyzed models including multispectral VIs as predictor reached R^2 values of <0.5. Therefore, multispectral VIs offered weak results in 2018 and 2019.

American Journal of Enology and Viticulture (AJEV). doi: 10.5344/ajev.2021.20063
AJEV Papers in Press are peer-reviewed, accepted articles that have not yet been published in a print issue of the journal or edited or formatted, but may be cited by DOI. The final version may contain substantive or nonsubstantive changes.

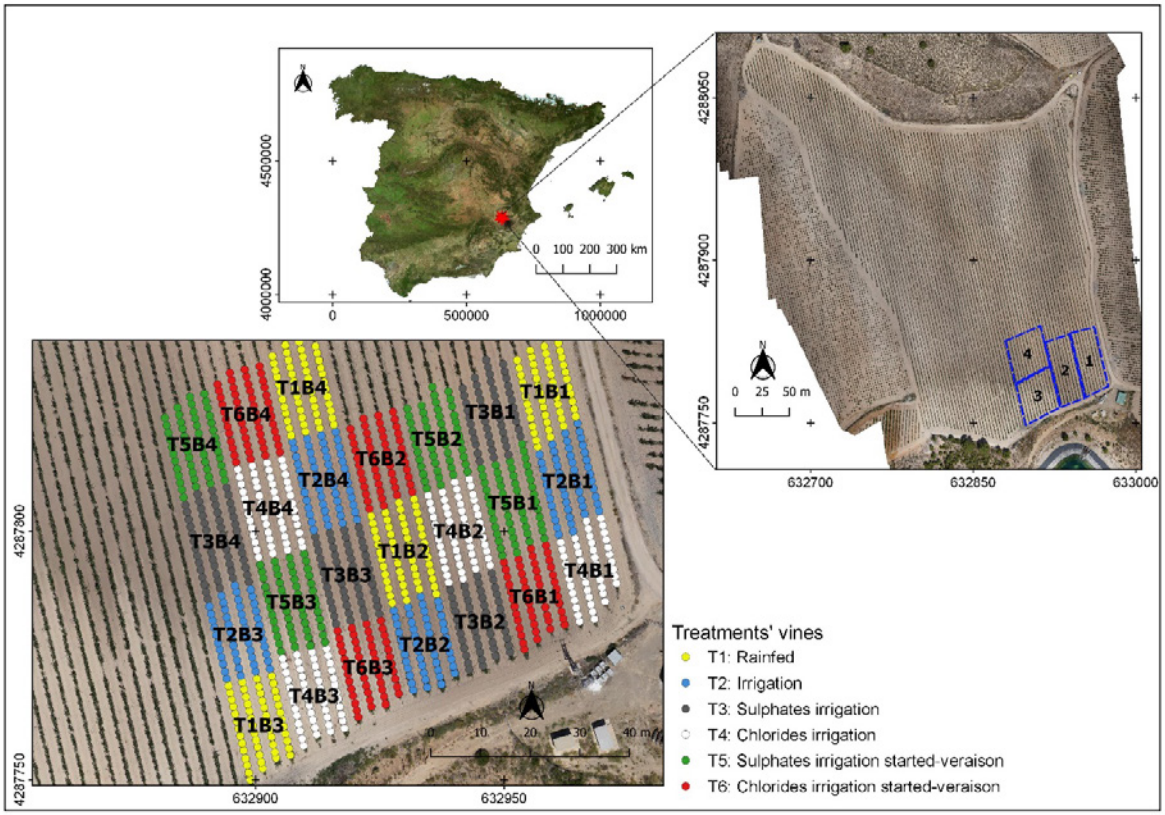

Figure 1 Location of the commercial vineyard cv. Monastrell in southeastern Spain, and replicate plot field distribution where the study was performed during 2018 and 2019 seasons. Each coloured dot corresponds to a grapevine plant.

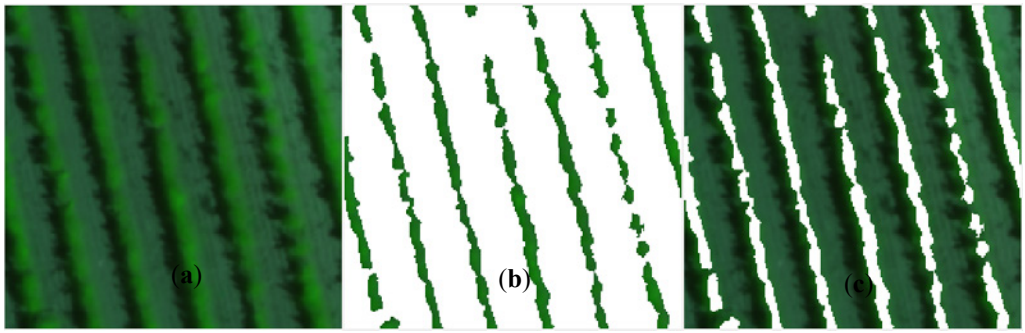

Figure 2 Three resulting images from well-illuminated vegetation segmentation with MS-GEO-LAIC, used for segmenting multispectral images: (**A**) the selected portion of the image; (**B**) the values of the pixels corresponding with the selected clusters; and (**C**) the values of the pixels corresponding to the unselected clusters.

American Journal of Enology and Viticulture (AJEV). doi: 10.5344/ajev.2021.20063
AJEV Papers in Press are peer-reviewed, accepted articles that have not yet been published in a print issue of the journal or edited or formatted, but may be cited by DOI. The final version may contain substantive or nonsubstantive changes.

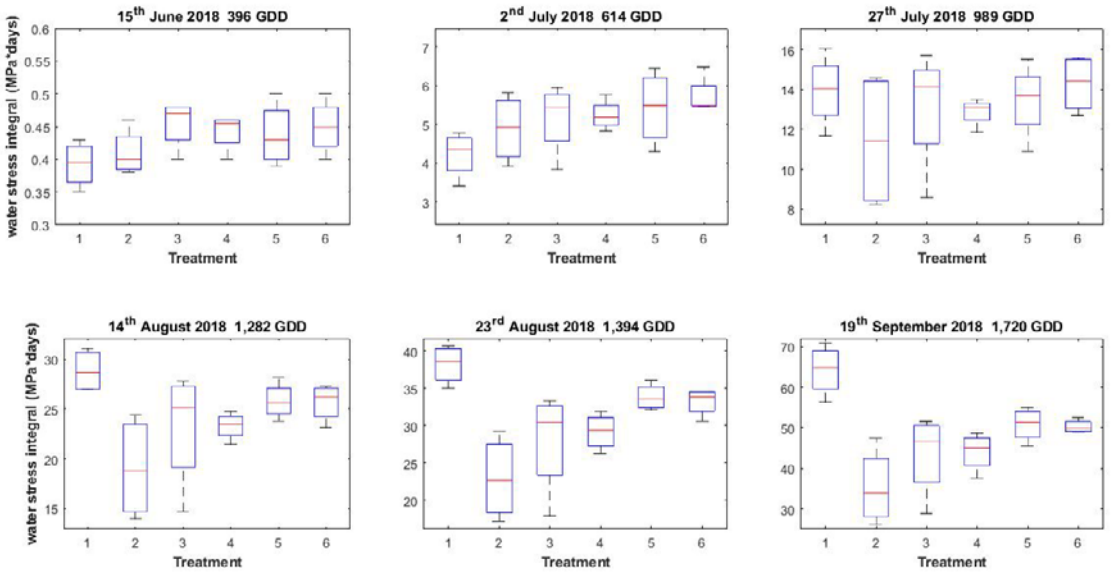

Figure 3 Water stress integral (MPa*days) of studied vineyard for different treatments of experimental design at different sampling dates in 2018 season.

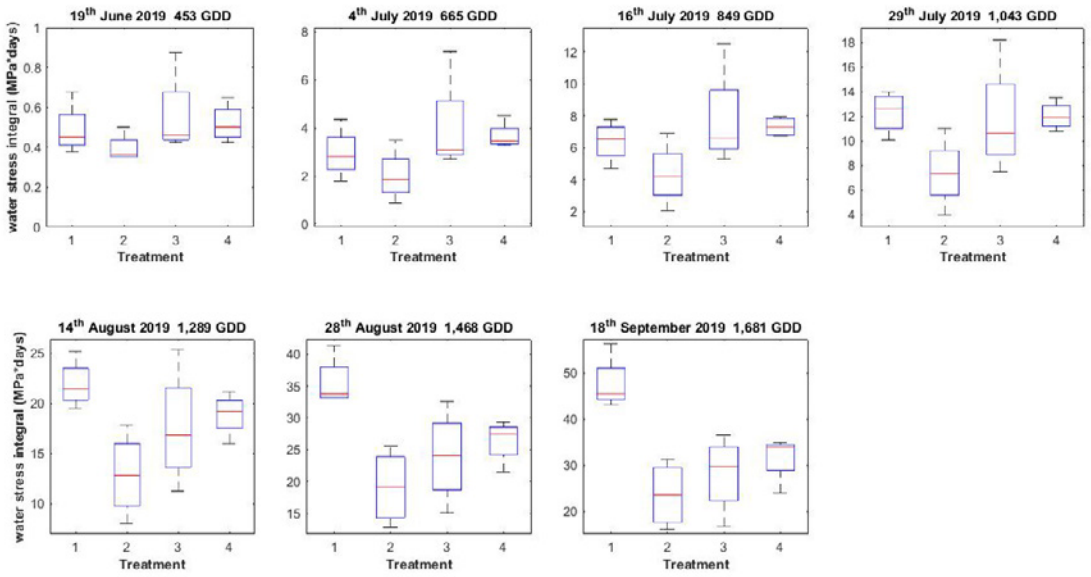

Figure 4 Water stress integral (MPa*days) of studied vineyard for different treatments of experimental design at different sampling dates in 2019 season.

American Journal of Enology and Viticulture (AJEV). doi: 10.5344/ajev.2021.20063
AJEV Papers in Press are peer-reviewed, accepted articles that have not yet been published in a print issue of the journal or edited or formatted, but may be cited by DOI. The final version may contain substantive or nonsubstantive changes.

a)

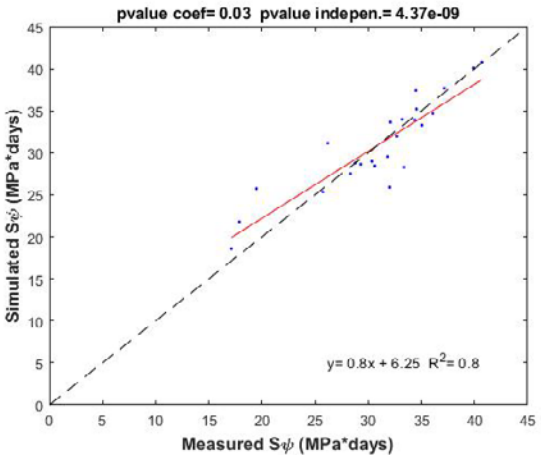

b)

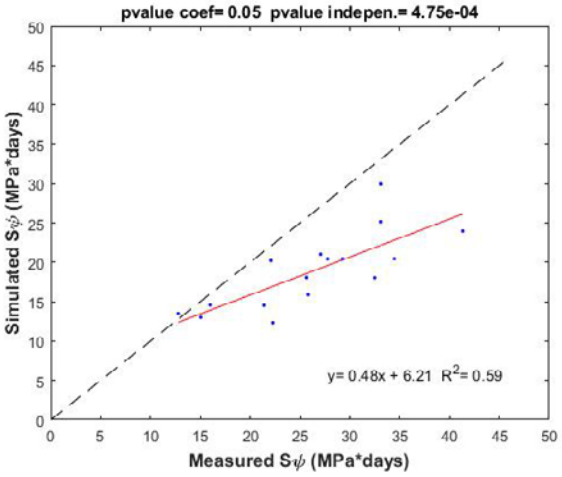

Figure 5 Regression line of: (**A**) measured Sψ and simulated Sψ with the calibrated model that used as predictor GLI data for 23rd August 2018 with 1,394 GDD, and (**B**) the validation process using the equation of the calibrated model with GLI data of 28th August 2019 with 1,468 GDD, similar to the calibrated model (1,394 GDD).